Journal of Hazardous Materials 424 (2022) 127696

Contents lists available at ScienceDirect

Journal of Hazardous Materials

journal homepage: www.elsevier.com/locate/jhazmat

Research Paper

Effect of sulfide on morphology and particle size of biologically produced elemental sulfur from industrial desulfurization reactors

Annemerel R. Mol [a,b], Lourens J. van Langeveld [b,c], Renata D. van der Weijden [a,d,*], Johannes B. M. Klok [a,b,d], Cees J.N. Buisman [a,d]

[a] Environmental Technology, Wageningen University & Research, P.O. Box 17, 6700 AA Wageningen, The Netherlands
[b] Paqell B.V., Reactorweg 301, 3542 AD Utrecht, The Netherlands
[c] Department of Earth Sciences, Utrecht University, Princetonlaan 8, 3584 CB Utrecht, The Netherlands
[d] Wetsus, European Centre of Excellence for Sustainable Water Technology, P.O: Box 1113, 8900 CC Leeuwarden, The Netherlands

ARTICLE INFO

Editor: Jianhua Guo

Keywords:
biodesulfurization
hydrogen sulfide
polysulfide
particle size analysis
settleability

ABSTRACT

We investigated the effect of polysulfide formation on properties of biologically produced elemental sulfur (S_8) crystals, which are produced during biological desulfurization (BD) of gas. The recent addition of an anoxic-sulfidic reactor (AnSuR) to the BD process resulted in agglomerated particles with better settleability for S_8 separation. In the AnSuR, polysulfides are formed by the reaction of bisulfide (HS^-) with S_8 and are subsequently oxidized to S_8 in a gas-lift reactor. Therefore, sulfur particles from the BD are shaped (i.e. morphology and particle size) both by formation and dissolution. We assessed the reaction of HS^- with S_8 particles in anoxic, abiotic experiments in a batch reactor using two S_8 samples from industrial BD reactors. Under these conditions, the sulfur particle surface became coarser and more porous, and in addition the smallest particles disappeared. Agglomerates initially fell apart but were reformed at a later stage. Moreover, we found different observed polysulfide formation rates for each S_8 sample, which was related to the initial morphology and size. Our findings show that particle properties can be controlled abiotically and that settleability of S_8 is increased by increasing both the HS^--S_8 ratio and retention time.

1. Introduction

Various types of microorganisms have the capacity to oxidize hydrogen sulfide (H_2S) to elemental sulfur (Ghosh and Dam, 2009). This oxidation reaction is particularly useful in technologies that desulfurize gas (González-Cortés et al., 2021; Buisman et al., 1990). Biological desulfurization (BD) technologies remove the toxic and corrosive H_2S from sour gas streams to produce clean gas, while simultaneously producing a commodity: elemental sulfur. Commercial users of these technologies prefer to produce elemental sulfur from the H_2S instead of sulfate or thiosulfate. Elemental sulfur is a solid and can therefore be easily separated from the process by sedimentation. Moreover the production of elemental sulfur does not lead to acidification of the process solution, as opposed to the formation of sulfate and thiosulfate, and the elemental sulfur is suitable to use as a fertilizer or fungicide (Janssen et al., 2001; Van Zessen et al., 2004; Fertipaq Natural Solutions, Fertipaq, 2021; Ceradis Crop Protection, 2021). Especially the small particle size and hydrophilicity of the biologically produced elemental sulfur are benefits for application.

In BD under halo-alkaline conditions (1 M Na^+, pH 8–9), the oxidation reaction is performed by chemolithoautotrophic sulfide oxidizing bacteria (SOB) that use O_2 as terminal electron acceptor (Eq. 1). Although the culture is open and mixed, the main thriving species in these reactors are of the genus *Thioalkalivibrio* (Kiragosyan et al., 2019; Muyzer et al., 2011; Sorokin et al., 2008; De Rink et al., 2019).

$$HS^- + ½O_2 \rightarrow S^0 + OH^- \quad (1)$$

Strict redox potential control is needed to prevent overdosing the microorganisms with O_2, which would lead to sulfate production (Janssen et al., 1998). Therefore, the main part of these reactors operates at very low O_2 concentration (Fig. 1). In addition, BD installations also have anoxic zones, such as the gas absorber. In these zones, sulfide is present, which originates from the sour gas stream. In the

* Corresponding author at: Environmental Technology, Wageningen University & Research, P.O. Box 17, 6700 AA Wageningen, The Netherlands.
E-mail addresses: annemerel.mol@wur.nl (A.R. Mol), l.j.vanlangeveld2@students.uu.nl (L.J. van Langeveld), renata.vanderweijden@wur.nl (R.D. van der Weijden), jan.klok@wetsus.nl (J.B.M. Klok), cees.buisman@wur.nl (C.J.N. Buisman).

https://doi.org/10.1016/j.jhazmat.2021.127696
Received 9 August 2021; Received in revised form 12 October 2021; Accepted 1 November 2021
Available online 7 November 2021

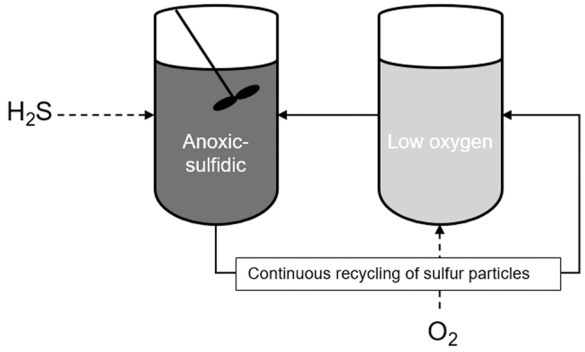

Fig. 1. Conceptual schematic of continuous recycling of sulfur particles over anoxic-sulfidic zone and low oxygen zone. In the anoxic-sulfidic zone, sulfur dissolution by polysulfide formation is the principal process. In the low oxygen zone, sulfur formation is the principal process.

anoxic-sulfidic zones, the produced elemental sulfur and the sulfide from the sour gas stream are mixed. The elemental sulfur is mainly present as cyclooctasulfur (S_8): rings of eight sulfur atoms. During this anoxic-sulfidic retention time, polysulfides are formed. This reaction has been described and studied in detail (Kafantaris and Druschel, 2020; Hartler et al., 1967; Avetisyan et al., 2019; Kleinjan et al., 2005a, 2005b; Kamyshny et al., 2004). Initially, the S_8 ring is opened by the strong nucleophile (species with an unshared electron pair, or Lewis base) HS^- (Kleinjan et al., 2005a) (Eq. 2). The resulting long chain polysulfides rearrange to shorter chain polysulfides by the reaction with another HS^- ion (Eq. 3).

$$HS^- + S_8 \leftrightarrows HS_9^- \leftrightarrows S_9^{2-} + H^+ \quad (2)$$

$$S_9^{2-} + HS^- \leftrightarrows 2\ S_5^{2-} + H^+ \quad (3)$$

Recently it was found that the sulfur particles change in size and morphology when the anoxic-sulfidic zone is extended by the addition of an anoxic-sulfidic reactor (AnSuR) in order to optimize the biological and process selectivity (De Rink et al., 2019; Kiragosyan et al., 2020). Particles formed in a set-up with an AnSuR are more agglomerated, the agglomerates have a stable and uniform size and moreover show good and stable sedimentation capacity. The agglomerates have a disorganized morphology, contrary to the often found smooth bipyramidal shaped crystals (Mol et al., 2021).

It is not clear what is causing this change in particle morphology and size. We want to unravel the effect of two processes that play a central role in the system: sulfur formation and sulfur dissolution. Regarding sulfur formation, the chemical species (S_x^{2-}in addition to HS^-) that are available to the microorganisms for oxidation influence the sulfur formation rate. With an approximated average polysulfide chain length of $x = 5$ under typical reaction conditions, S_8 production rate from polysulfide is expected to be at least 5x higher than from sulfide (Roman et al., 2014). This is supported by two studies that indicated that biological oxidation of polysulfide takes place at a higher rate than the biological oxidation of sulfide and is not limited by higher concentrations of polysulfide (Banciu et al., 2004; Van Den Bosch et al., 2009). In addition, a shift in microbial population due to the applied conditions might lead to a higher abundance of species with different sulfur metabolisms, which could influence the rate of sulfur formation (Sorokin et al., 2003). The sulfur formation rate is expected to influence the degree of elemental sulfur supersaturation, which has a strong impact on the size and morphology of the sulfur particles. Concerning sulfur dissolution, the reaction of HS^- and S_x^{2-} at the surface of the sulfur particles might also drastically change the morphology and particle size. Especially the surface properties (e.g. roughness, hydrophilicity) are expected to change as a result of sulfur dissolution. The nucleophilic dissolution rate of elemental sulfur depends on the specific surface area. The specific surface area is thus rate determining for polysulfide formation (Kafantaris and Druschel, 2020; Avetisyan et al., 2019; Kleinjan et al., 2005a; Kamyshny et al., 2003). Part of the smallest sulfur particles can also completely dissolve in the AnSuR depending on the operational conditions such as H_2S loading rate and retention time in the AnSuR (Mol et al., 2021).

In this study, we performed batch reactor experiments to assess the effect of sulfide addition on the sulfur particle morphology and size distribution in an anoxic environment. With these experiments we separated the sulfur dissolution step from the biological formation step. Thus, in this study we investigated the contribution of only the dissolution reaction on the sulfur particle properties. We reported changes in particle size and morphology at different polysulfide formation rates for two different industrial BD sulfur samples. Moreover, the reaction of elemental sulfur with (poly)sulfide changed surface properties of the particles. The different results in particle size distribution (PSD) and morphological development and polysulfide formation rate for the elemental sulfur samples appear to be related to the initial shape and size of the particles. The results of this study address the effect of increasing the anoxic zone and can help to control sulfur particle properties to increase their settleability in BD technology.

2. Materials and methods

2.1. Chemicals used

Experiments were performed in a solution with conditions that are typical for the BD process. A buffer solution was prepared by adding 6.67 Na_2CO_3 and 69.4 $NaHCO_3$ gram (analytical grade) per liter distilled water and had a pH of 8.52 and conductivity of 51.9 mS cm^{-1} at 35 °C. This buffer solution was used to prepare elemental sulfur suspensions, polysulfide stock solutions and sulfide stock solutions. Sulfide stocks were prepared by adding hydrated sodium hydrosulfide salt ($NaHS{\bullet}xH_2O$) to 100 mL of the buffer solution. We used a hydrated form of the sodium hydrosulfide salt because anhydrous sodium hydrosulfide hydrolyzes by atmospheric moisture to H_2S. The hydrated form is more stable. $NaHS{\bullet}xH_2O$ was used instead of Na_2S because it is more pH neutral. During the experiments, two stocks were used of approximately 0.2 and 0.4 M HS^-. For these stocks 1.5124 g and 2.9650 g were dissolved in approximately 100 mL buffer solution. Prior to adding the hydrosulfide salt, the buffer solution was flushed for at least 10 min with nitrogen gas (N_2) to remove most of the dissolved oxygen. The sodium hydrosulfide stock was kept in an air-tight batch bottle with rubber stopper. Before each experiment, the concentration of the bisulfide stock was determined by titration with a solution of 0.1 M $AgNO_3$, using a Titrino Plus Titrator (Metrohm, Herisau, Switzerland) (De Rink et al., 2019). The titration was performed by adding 100 µL sulfide stock to 80 mL NaOH (5%) and 10 mL NH_3 (2.5%) to stabilize the dissolved sulfide. Polysulfide (S_x^{2-}) standards for spectrophotometric analysis were prepared by adding elemental sulfur (chemically produced analytical grade) to an excess (molar S ratio of 1:10) of $NaHS{\bullet}xH_2O$ in the buffer solution. The resulting solution was placed in a shaker at 35 °C until all elemental sulfur was visibly dissolved to S_x^{2-}. Based on the concentration of elemental sulfur in the solution, the total amount of zero-valent sulfur atoms in polysulfide ions [S^0 in S_x^{2-}] was 76 mM. Calculation with OLI Studio (OLI Systems, Inc. Cedar Knolls, NJ, USA) showed that this is equal to a total polysulfide concentration of 23.5 mM. However, this is an underestimation as OLI Studio did not include S_6^{2-} and S_7^{2-}. This concentrated S_x^{2-} solution was diluted with N_2 flushed buffer in air-tight batch bottles to S_x^{2-} standards with intended concentrations of 0.2, 0.4, 0.6, 1.0 and 2.0 mM S^0 in S_x^{2-}. A batch bottle was filled with buffer solution, flushed with N_2 and weighed. A needle and syringe were flushed with N_2, with which subsequently a small volume was taken from the concentrated polysulfide stock and added to the batch bottle. The plunger of the syringe was moved up and down three times to flush the syringe with buffer before it was removed from the batch bottle. The flushing made sure that all concentrated

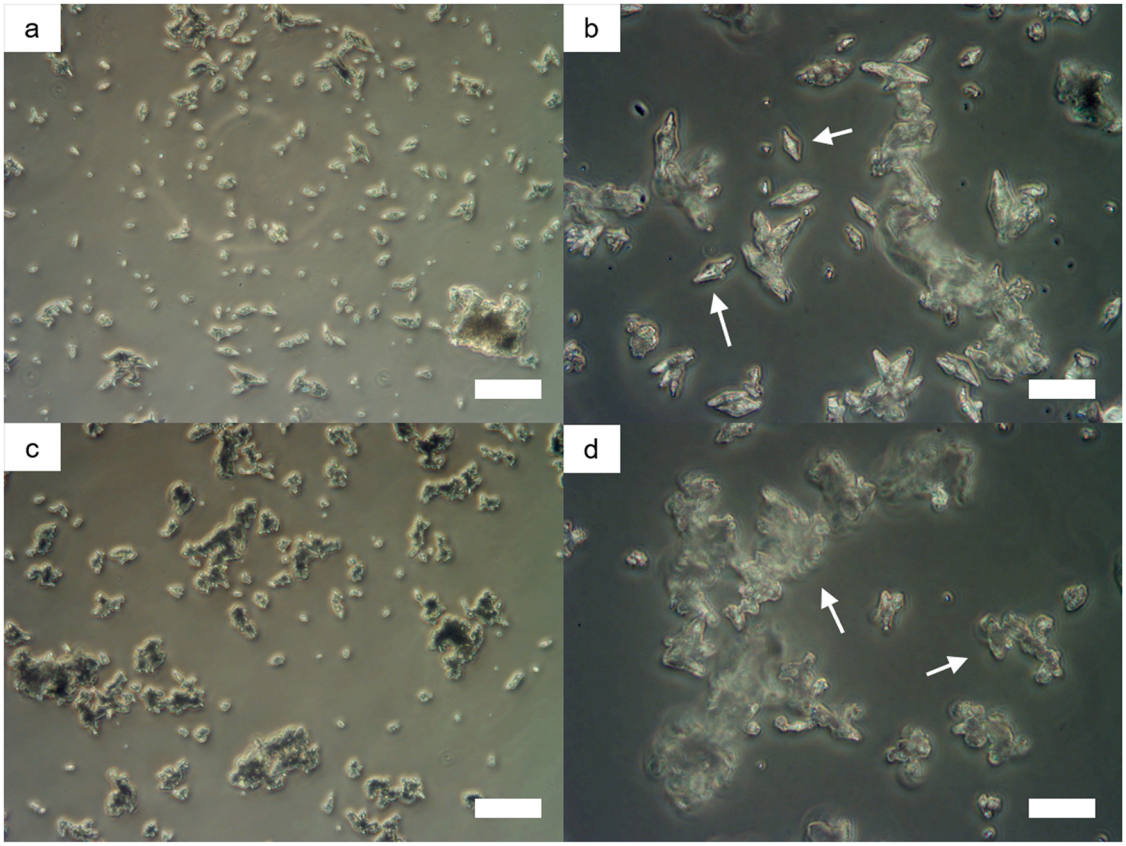

Fig. 2. Light microscopy pictures of biologically produced sulfur from PM1 (a, b) and PM2 (c, d) at 400× (a, c; scale bar right bottom of each picture: 50 μm) and 1000× magnification (b, d; scale bar: 20 μm). White arrows indicate single crystals (b) and agglomerates (d).

polysulfide stock ended up in the batch bottle. After addition, the batch bottle was vigorously shaken to make sure the solution was properly mixed. Then, the bottle and content were weighed again to know exactly how much concentrated polysulfide stock was added. Exact concentrations of the standards and their linear calibration curve are reported in the Supplementary Information (SI Table 1 and SI Fig. 1).

For the experiments simulating the AnSuR, biologically produced sulfur was obtained from two different industrial BD facilities in the Netherlands: paper factory SCA (now Essity) in Cuijk, hereafter called 'Paper mill 1' (PM1) and wastewater treatment plant Industriewater Eerbeek in Eerbeek, hereafter called 'Paper mill 2' (PM2) (Janssen et al., 2009; Mol et al., 2020). The obtained sulfur suspensions were washed to remove salts and microorganisms. The washing procedure was performed by centrifuging the suspension, discarding the supernatant and layer with microorganisms on the sulfur pellet and resuspending the sulfur pellet with distilled water. These steps were repeated until the supernatant conductivity was below 1 mS cm^{-1}. Subsequently, the sulfur was dried overnight at 50 °C. Then, a 1 L suspension was prepared by weighing the dried sulfur and adding buffer solution. The suspension was stirred with a magnetic stirrer overnight to completely suspend the sulfur and to break down any attachments that were formed as a result of drying the sulfur. Prior to the dissolution experiments, the biologically produced sulfur from two industrial BD installations was characterized by light microscopy (Fig. 2). For PM1, the particles had a defined bipyramidal crystal habit, which is typical orthorhombic α-S_8 (Fig. 2a, b). PM2 appeared more agglomerated and particles in the sample lacked a defined crystal shape (Fig. 2c, d).

2.2. Analysis

Sulfur particle size distribution (PSD) was analyzed using laser diffraction (SALD-2300, Shimadzu, Kyoto, Japan) with a refractive index of 2.0 for α-S_8 (Mol et al., 2020; Lide, 2005). Laser diffraction is a commonly used technique to measure PSD in the size range of the particles in our study. In our previous study, we have shown that PSD is a representative parameter to assess differences in sulfur particle sizes (Mol et al., 2020). For calculations of PSD, the software from the laser diffraction itself was used (WingSALD-II, Shimadzu, Kyoto, Japan). Sulfur particle morphology was analyzed with a Nikon Eclipse E400 light microscope (Nikon, Tokyo, Japan) and pictures taken with an Euromex CMEX 18-PRO camera (Euromex Microscopen bv, Arnhem, The Netherlands). In addition, Scanning Electron Microscopy (SEM) was used to analyze particle morphology. The pictures from Fig. 5 were taken with a Phenom XL G2 Desktop SEM (Thermo Fisher Scientific, Waltham, Massachusetts, USA). The samples were mounted on carbon adhesive tabs and analyzed at 10 kV and 60 Pa. The pictures from Figs. 9–10 were taken according to (Mol et al., 2020). Particle composition was studied by X-ray diffraction (XRD) according to (Mol et al., 2020). The concentration of polysulfide was determined spectrophotometrically at $\lambda = 285$ nm. At this wavelength, the concentration of zerovalent sulfur atoms in S_x^{2-} ([S^0 in S_x^{2-}]) can be determined, approximately independent of pH and the ratio between [S^0 in S_x^{2-}] and [S^{2-}] (Teder, 1967; Danielsson et al., 1996). The device used was a Tecan Infinite M200 Pro (Tecan Group ltd., Männedorf, Switzerland) that equipped Hellma Type 100-QS quartz cuvettes of 10 mm in diameter (Hellma GmbH & Co. KG, Müllheim, Germany). Calibration over a time span of 4.5 months showed a stable single of the UV lamp (SI Fig. 2), which eliminated the necessity of performing time-consuming re-calibration each time polysulfide analyses were performed. Samples were filtered through a 0.20 μm cellulose acetate membrane filter to remove elemental sulfur particles, after which they were diluted 10x with N_2 flushed buffer. The time between sampling and spectrophotometric

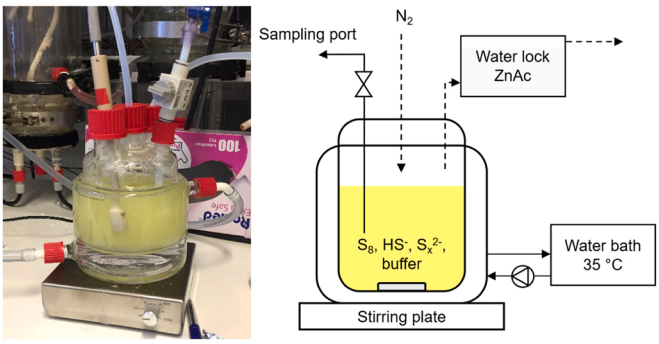

Fig. 3. Picture (left) and schematic drawing (right) of batch reactor set-up.

analysis was kept as short as possible to prevent oxidation with air of the (poly)sulfides. Maximum observed S_x^{2-} formation rates were calculated by applying a linear relation to (at least) three S_x^{2-} concentration data points that formed the steepest slope in the sample's dataset. These rates were used as an indication of the relative formation rates of polysulfides between samples. Both the first order reaction rate (Eq. 2) and the autocatalytic reaction rate (Eq. 3) contributed to the total observed polysulfide formation rate.

2.3. Experimental set-up

The set-up consisted of a 250 mL glass reactor with a double glass wall connected to a water bath with a thermostat at 35 °C (Fig. 3). The reactor liquid was actively stirred by a magnetic stirring bar at a constant rate of 100 rpm. Samples were taken through a sampling port with a syringe. The lowest point of the sampling port was positioned halfway into the reactor liquid to obtain a representative sample. After sampling, leftover liquid in the sampling port was pushed back into the stirred reactor with a syringe filled with N_2. Subsequently, a valve in the sampling was closed to secure that no O_2 diffused into the reactor. In addition, there was an inlet for N_2 flushing, which provided light overpressure inside the reactor to prevent O_2 diffusion into the reactor liquid as well. A water-lock containing a saturated solution of zinc acetate kept the system airtight and free of pressure build-up. Zinc captured any potentially released H_2S. All ports were closed off airtight by a screwcap with a septum fitted to the tubing going through it.

2.4. Experimental design

A total of 10 batch reactor experiments were performed: five for each industrial sulfur sample (Table 1). To follow the reaction of biologically produced sulfur with sulfide in detail, a high sampling frequency and direct sample analysis were needed. Separated experiments were dedicated to i) assess the change in morphology and size distribution of the biologically produced sulfur particles upon addition of sulfide (PM1:1–2 and PM2:1–2) and ii) to estimate polysulfide formation/sulfur dissolution rates by spectrophotometric analysis of polysulfide concentration (PM1:3–5 and PM2:3–5). The concentrations of biologically produced sulfur and sulfide were based on ratios applied in industry (De Rink et al., 2019; Roman et al., 2014). In addition, three experiments (PM1:2 and PM2:1–2) were performed with an excess of sulfide in the process solution.

2.5. Experimental operation

The bottle with sulfur suspension was shaken to homogenize the suspension and subsequently the suspension was poured in the batch reactor. The reactor content was flushed for 30 min with N_2 to create anoxic conditions. After flushing, a time zero-measurement sample was taken from the reactor. For the PSD and morphology experiments, the PSD and morphology were analyzed directly after sampling. For the polysulfide formation experiments, the polysulfide concentration was also measured directly after sampling. After the time zero-measurement, sulfide stock solution was injected to initiate the reaction, which marked the start of the experiment. Five minutes after sulfide injection, another

Table 1
Experimental conditions applied to study particle size distribution and morphology development and/or polysulfide formation rates.

	PSD + morphology				PSD + polysulfide formation					
Experiment	PM1: 1	PM1: 2	PM2: 1	PM2: 2	PM1: 3	PM1: 4	PM1: 5	PM2: 3	PM2: 4	PM2: 5
[HS^-] (mM)	9.2	13.9	13.8	13.8	6.0	5.5	10.4	6.0	5.5	5.6
[S^0-S_8] (mM)	27.3	14.2	14.0	14.1	28.8	28.9	28.5	29.4	29.0	29.0
Sulfide-sulfur ratio	0.3	1.0	1.0	1.0	0.2	0.2	0.4	0.2	0.2	0.2

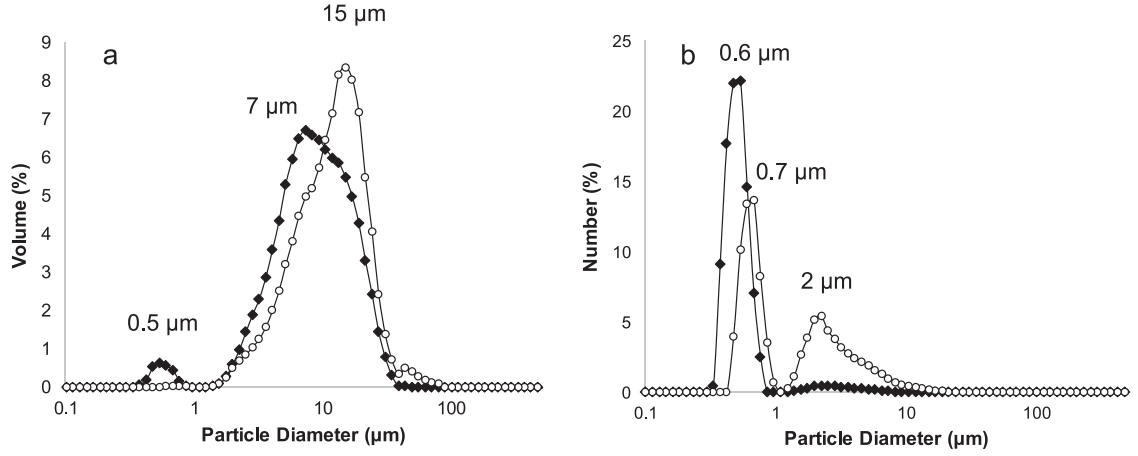

Fig. 4. Volume- (a) and number- (b) based particle size distributions of PM1 (◆) and PM2 (o). Triplicate measurements showed good reproducibility with average ranges of 0.02% (PM1 volume-based), 0.03% (PM2 volume-based), 0.03% (PM1 number-based) and 0.25% (PM2 number-based). Modal particle diameters are indicated in the figures.

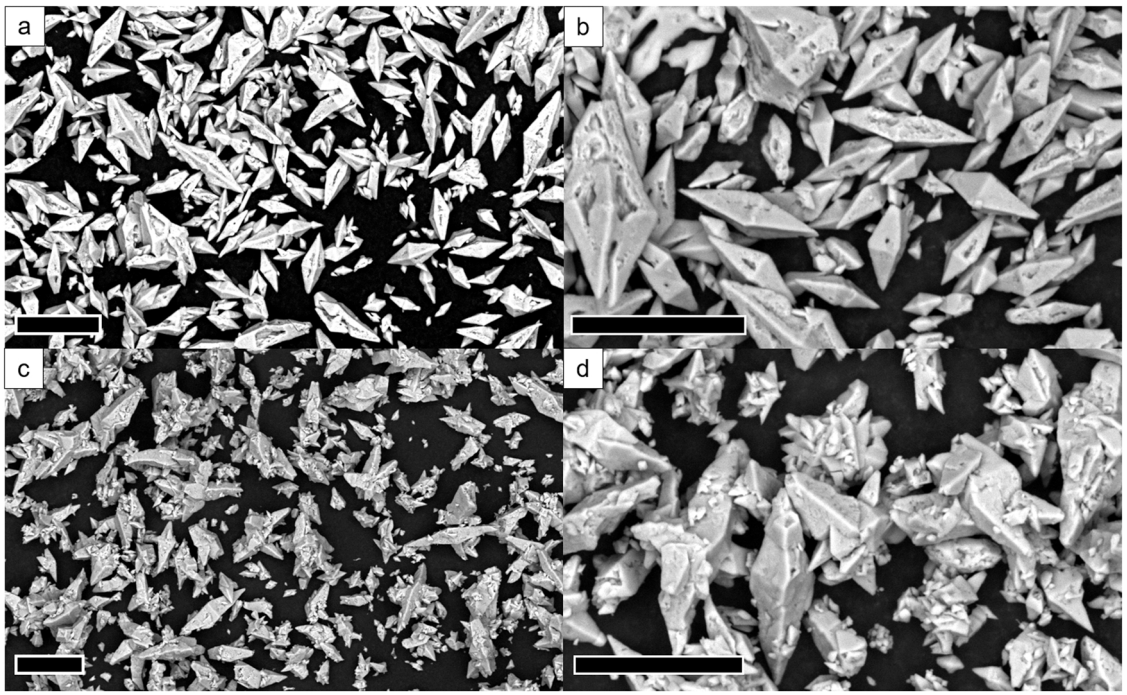

Fig. 5. Scanning Electron Microscopy pictures of biologically produced elemental sulfur from PM1 (a-b) and PM2 (c-d). Scale bars: 20 μm.

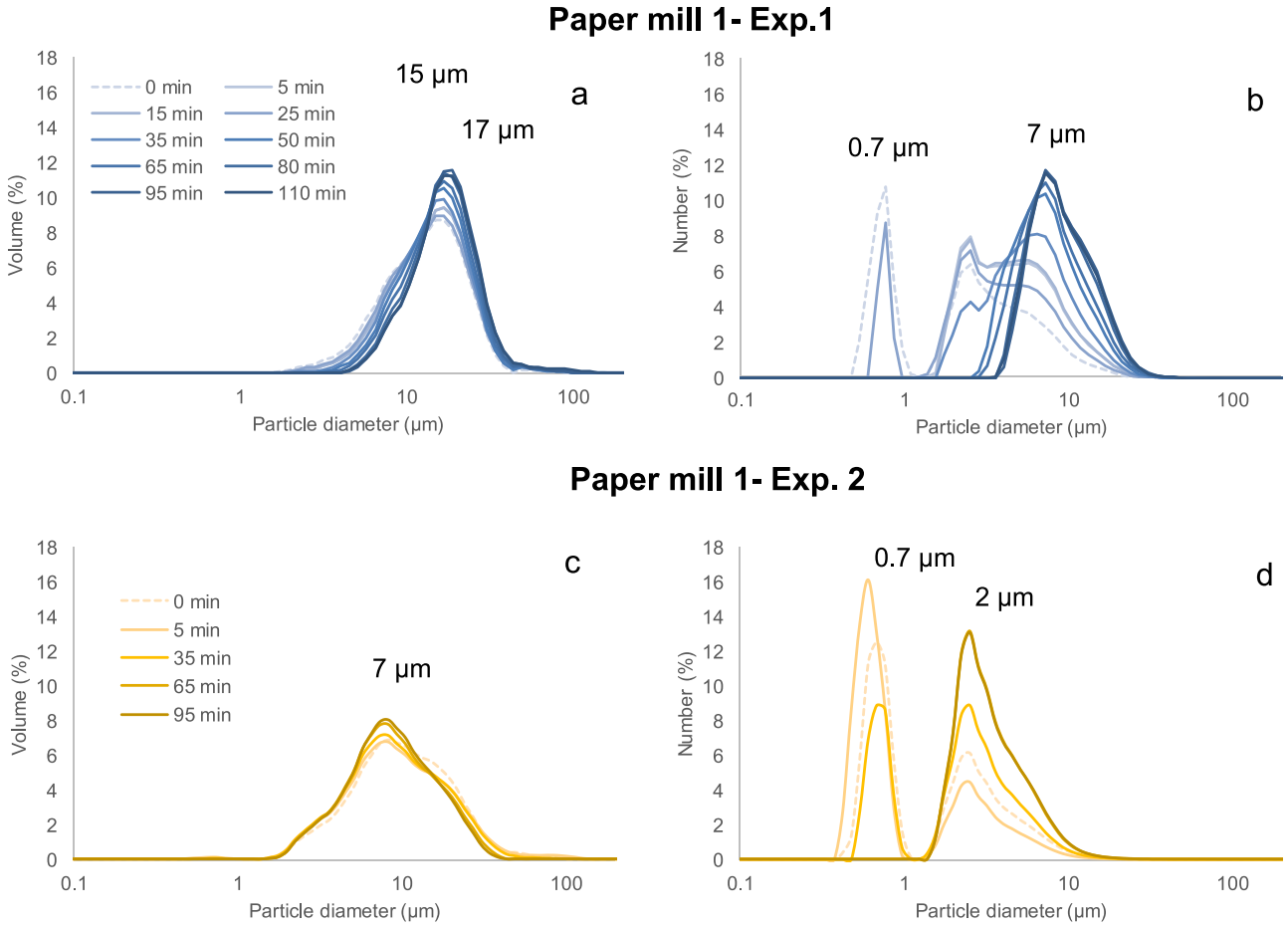

Fig. 6. Development of volume- (a, c) and number- (b, d) based particle size distribution of Paper mill 1 after addition of sulfide in two different sulfur: sulfide ratios (PM1:1; 0.3 and PM1:2; 1.0).

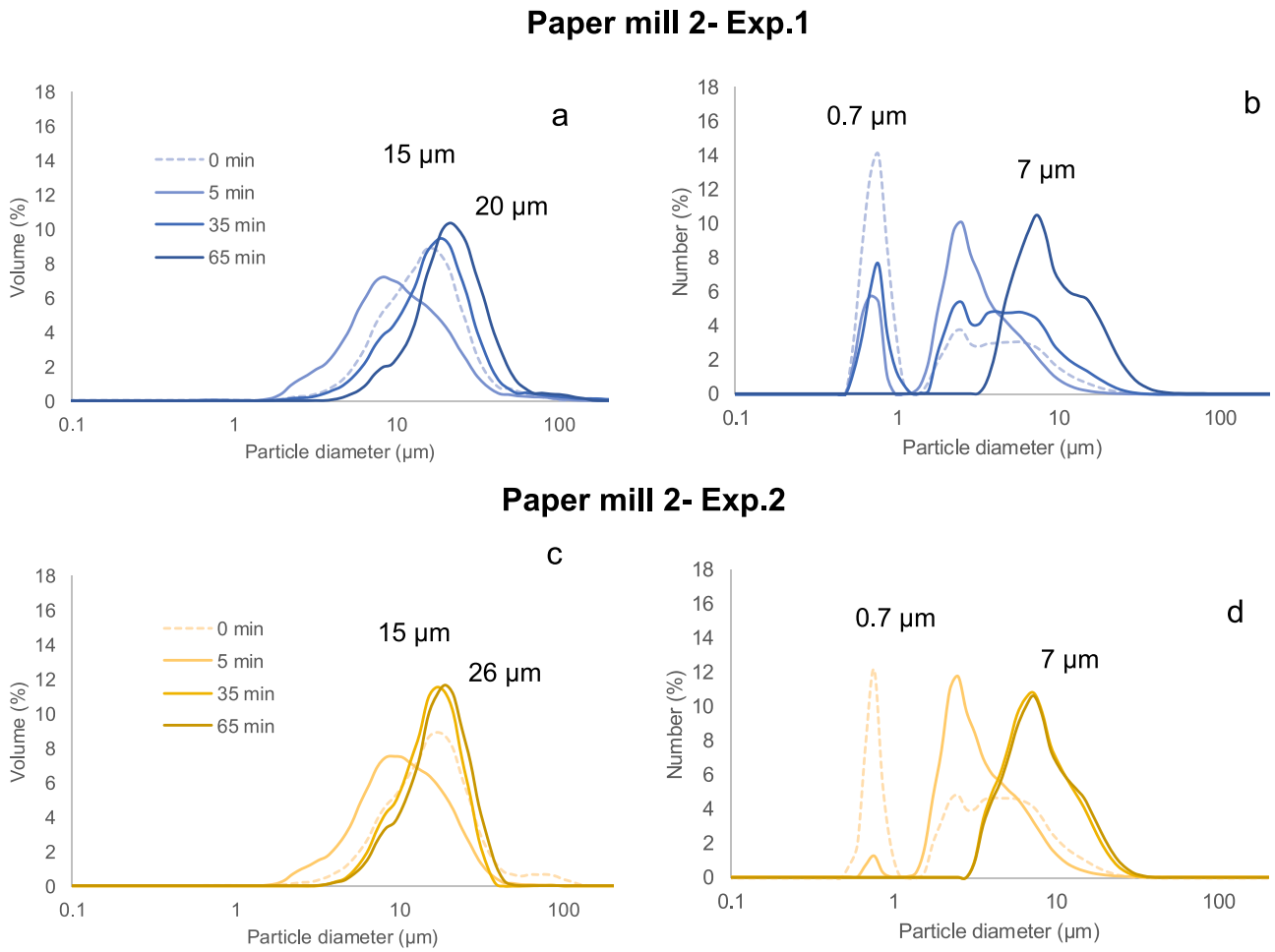

Fig. 7. Development of volume- (a, c) and number- (b, d) based particle size distribution of Paper mill 2 after addition of sulfide at a sulfur-sulfide ratio of 1.0 (PM2:1 and PM2:2).

sample was taken. For the remainder of the experiment, samples were taken every 30 min for the PSD and morphology experiments and every 10–15 min for the polysulfide formation experiments. The PSDs of the time zero-measurement of PM1:1 and PM2:3 contained some larger particles than the other time zero-measurements, due to improper mixing of the sulfur stock suspension before loading the batch reactor. As a result, some larger particles remained in the last 200 mL of suspension in the bottle. The number-based distributions for PM2 also varied a little (SI Figs. 8–10), but unfortunately, we do not have a clear explanation for this. However, we argue that this discrepancy does not influence our main conclusions as the trends in PSD change are still the same as in the other experiments.

3. Results

3.1. Detailed characterization of biologically produced elemental sulfur

Prior to the dissolution experiments, the biologically produced elemental sulfur samples from the industrial BD installations were further characterized. The volume-based modal diameters for Paper mill 1 (PM1) and Paper mill 2 (PM2) were 7 µm and 15 µm (Fig. 4a). Furthermore, a small peak was observed in PM1 at 0.5 µm, which comprised 3% of the volume of the sulfur. These particles all had a diameter <1 µm. In PM2 these particles only comprised 0.2% of the volume. The number-based modal diameters were similar: 0.6 and 0.7 µm (Fig. 4b). For PM1 almost all particles (96%) were <1 µm. For PM2 also a peak was found with a modal diameter of 2 µm. Therefore, for PM2 only 54% of the particles was <1 µm.

In addition, detailed morphological differences were observed between the biologically produced sulfur particles (Fig. 5). The differences between the samples as observed by light microscopy and SEM agreed with the PSD: PM1 contained mostly bipyramidal single crystals and PM2 contained predominantly agglomerates. The bipyramidal crystals from PM1 were 1–25 µm in length and 1–10 µm in width. The crystals either had smooth crystal facets or a hollow 'hoppered' shape (Desarnaud et al., 2018). Some crystals appeared broken at either the corners or in the middle of the crystal halfway through. From some crystal surfaces another crystal appeared to be growing. This growth process could have led to a type of crystal twinning or skeletal hopper growth, where two bipyramids were connected either at a facet or at a corner.

The agglomerates from PM2 were up to 40 µm in size, although the boundaries of the agglomerates were difficult to distinguish in the SEM pictures. Some small loose crystals and crystal fragments were present in the sample as well. The agglomerates seemed to have predominantly formed by the growth of crystals on the facets of other crystals. No hopper growth was observed in PM2. From the SEM pictures it also seems that the specific surface area of PM2 is higher than that of PM1 since the agglomerates are composed of many small particles.

The crystal structure of the two samples was analyzed with powder-XRD. Both samples were identified as orthorhombic α-S_8 (SI Fig. 3). The crystallinities as calculated with the XRD software were almost identical: 92.3% for PM1 and 91.6% for PM2. Moreover, no significant differences were found between the crystallite sizes (smallest single crystals) of the sulfur crystals from both samples.

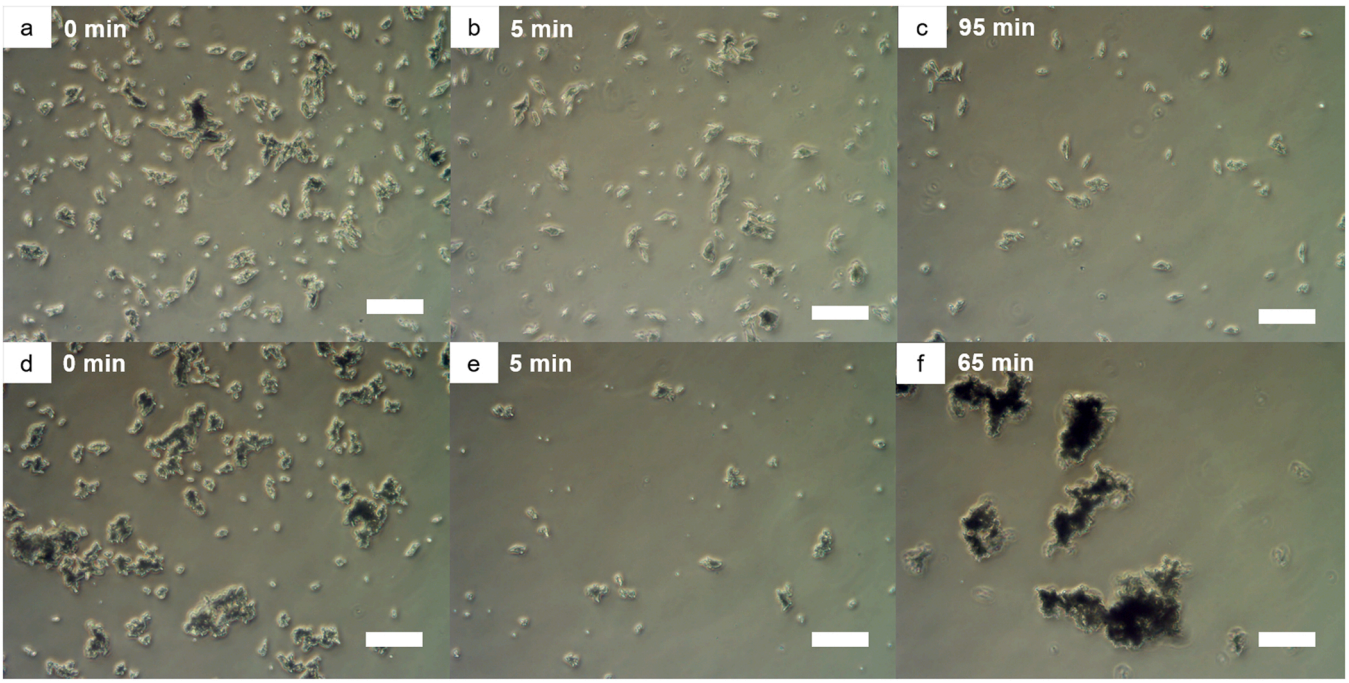

Fig. 8. Light microscopy pictures of PM1:2 at time 0 min (a), 5 min (b) and 95 min (c) and PM2:2 at time 0 min (d), 5 min (e) and 65 min (f). Scale bar: 50 μm.

3.2. Batch reactor experiments

3.2.1. Particle size and morphology development

After characterization, the sulfur particles in a buffer solution were exposed to sulfide. Their PSD and morphology were analyzed during the first four experiments (PM1:1–2 and PM2:1–2). In general, we found that the smallest particles were no longer detected when sulfide was added to the experiments. This result was found for both biologically produced elemental sulfur samples (Figs. 6–7). For PM1 the shift in PSD was most evident for the number-based distributions (Fig. 6b, d). The modal particle diameters gradually shifted from 0.7 to 2 and 7 μm. For PM1:1 at time 0 min, 65% of the particles was smaller than 3.2 μm. After 110 min, no more particles were present below 3.2 μm. For PM1:2 the results were comparable; at time 0 min 50% of the particles was smaller

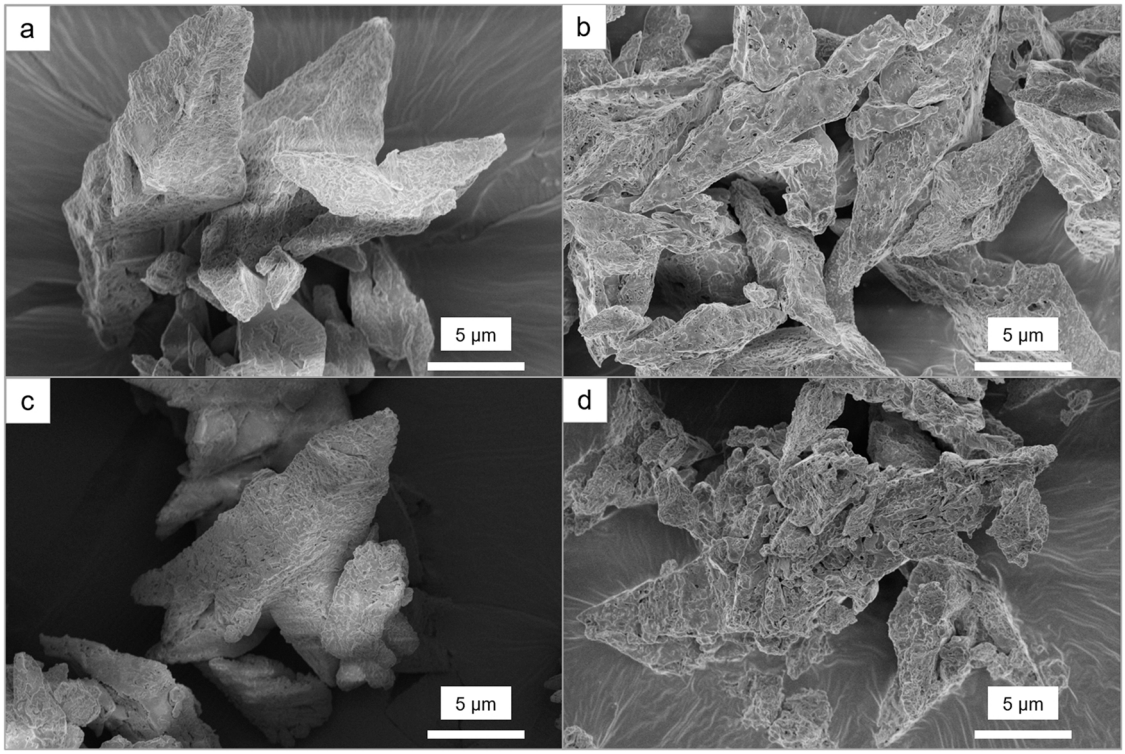

Fig. 9. Surface of elemental sulfur particles before (a, c) and after (b, d) dissolution with HS^-. After dissolution the surface appears coarser and more porous. PM1: a-b, PM2: c-d.

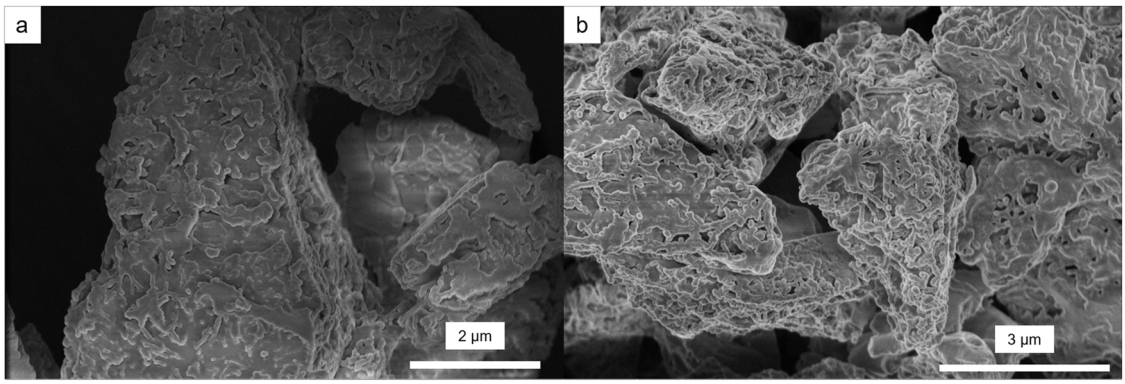

Fig. 10. Detail of surface of PM2 before (a) and after (b) dissolution with HS^-.

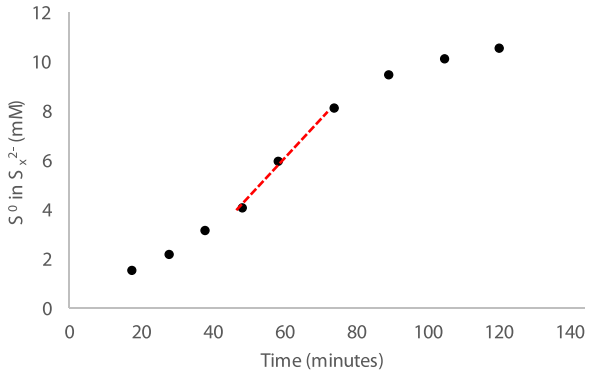

Fig. 11. Polysulfide formation during PM1–1. The maximum observed rate was estimated from the steepest part the curve indicated by the red dashed line.

than 1 µm, but at time 95 min no particles smaller than 1 µm were detected anymore. Regarding the volume-based distributions, only a slight shift in particle size was observed (Fig. 6a, c).

For PM2 the modal diameters also shifted from 0.7 to 7 µm for the number-based distribution (Fig. 7b, d). At time 0 for PM2:1 50% and for PM2:2 67% of the particles were smaller than 3 µm. After 65 min, all these particles had disappeared. For the volume-based distribution also a shift in particle size was observed. The modal particle diameters shifted from 15 to 20 and 26 µm. A remarkable shift in particle size was observed in the PSD of PM2:1 and 2 (Fig. 7a, c). At 5 min the peak shifted to the left as the bulk of the particles became smaller, but at 35 and 65 min the peak moved to the right again as the bulk particle size increased.

To clarify the PSD observations, light microscopy pictures were taken at the various time points (0, 5 and 65 or 95 min) of the experiments. The samples consisted of both loose particles and agglomerates particles. In general, the agglomerated particles disappeared during the experiments. Instead, loose particles were observed, that either stayed loose or re-agglomerated. Specifically, for PM1:2 (Fig. 8a-c) the agglomerates at the start of the experiments (0 min) had completely disappeared at the end of the experiment at 95 min. In addition, at 95 min the smallest particles were also no longer visible (Fig. 8c), which agrees with the PSD (Fig. 6d). Similarly, for PM2:2 (Fig. 8d-f) particle agglomeration decreased, but after 65 min agglomerates were observed again. The agglomerates detected after 65 min are larger and denser than the agglomerates observed at 0 min. This 're-agglomeration' agreed with the observed changes in PSD. In addition, like in PM1:2, also in PM2:2 the smallest particles were absent at the end of the experiment. Light microscopy pictures of PM2:1 showed comparable results (SI Fig. 4).

The surface structure of the elemental sulfur particles also changed due to the dissolution reaction with HS^- (Fig. 9). For both samples, the surface appeared coarser and more porous at the end of the experiment, although the surface of the untreated elemental sulfur samples was also quite rough. Especially the surface of PM2 appeared much rougher (Fig. 10b): a network of globules (100–200 nm) became visible. This structure was also visible in the untreated sample, but not as explicitly (Fig. 10a).

Table 2
Maximum observed polysulfide formation rates for the polysulfide formation experiments.

Experiments	Sulfide-sulfur ratio	$\%S_0$ in S_x^{2-} in equilibrium	Maximum observed S_x^{2-} formation rate (mM min^{-1})	Average maximum observed S_x^{2-} formation rate (mM min^{-1})
PM1:1	0.3	28	0.159	0.08
PM1:2	1.0	80	n.a.	
PM1:3	0.2	17	0.036	
PM1:4	0.2	16	0.037	
PM1:5	0.4	30	0.108	
PM2:1	1.0	81	n.a.	0.15
PM2:2	1.0	80	n.a.	
PM2:3	0.2	17	0.202	
PM2:4	0.2	16	0.086	
PM2:5	0.2	16	0.180	

3.2.2. *Polysulfide formation*

During each experiment, polysulfide was formed by the reaction of sulfide with elemental sulfur particles. In experiments 3–5 of both samples and experiment 1 of PM1 the polysulfide concentration was measured spectrophotometrically. Maximum observed polysulfide formation rates were estimated from the measured polysulfide concentrations. A typical S-curve for the autocatalytic formation of polysulfides was observed (Fig. 11).

The rates indicated the relative polysulfide formation rate per sample. For PM1 the rates ranged from 0.036 to 0.159 mM min^{-1} with an average of 0.08 mM min^{-1} (Table 2). The rates of PM2 were on average almost two times higher; they ranged between 0.086 and 0.202 mM min^{-1} with an average of 0.15 mM min^{-1}.

For these experiments the PSD was also analyzed. However, the sulfide-sulfur ratio was too low to observe any changes in PSD (SI Figs. 5–10). For the low sulfide-sulfur ratio, 16% of the elemental sulfur was converted to polysulfide. For the high sulfide-sulfur ratio this was 80%. Only in experiment PM1:5 the PSD changed and followed a similar pattern as the PSD from experiment PM1:1 (SI Fig. 7). Likely the pattern was the same because of the similar sulfide-sulfur ratio (0.4, 30% of the elemental sulfur to polysulfide).

4. Discussion

In a previous study, we found that the properties of the produced elemental sulfur particles changed by addition of an AnSuR to the BD process (Mol et al., 2021). Due to this environment, the particles were more agglomerated and had a disorganized structure. Up to now, the effect of the nucleophilic dissolution reaction on the particle properties was not clear, as the changed particle properties could also result from a combination of the sulfur formation and dissolution. Therefore, we assessed the effect of sulfide addition on elemental sulfur particle size distribution (PSD) and morphology in an anoxic, sulfidic environment in this study. In line with our hypothesis, we found that dissolution of elemental sulfur by (poly)sulfide changed the PSD and morphology. Hereby we show that these changes are caused by abiotic reactions between sulfur and (poly)sulfide only, i.e. not caused by biological (poly)sulfide oxidation. Moreover, we discovered for each sample a different observed maximum polysulfide formation rate which is related to the difference in the initial morphology and size distribution.

In experiment 1–2 for both samples (3 out of 4 with high sulfide-sulfur ratio), PSD gradually changed after the addition of sulfide. In general, the modal particle size increased because the smallest particles (below 1 or 3 μm) disappeared (Figs. 6–7). In contrast, in the experiments with the lowest sulfide-sulfur ratio, little change in PSD occurred (SI Figs. 5–10). Whether the dissolution caused a change in particle properties was thus dependent on the sulfide-sulfur ratio. Moreover, the changes were gradual. This meant that before equilibrium was reached, only a certain amount of the total elemental sulfur was converted to polysulfide. We calculated that for the experiments with a sulfur: sulfide ratio of 1, when equilibrium was reached, 80% of the elemental sulfur was present as polysulfide. For the experiments with a sulfide-sulfur ratio of around 0.2, this was only 16% in equilibrium. The dependence on the sulfide-sulfur ratio and reaction time has far-reaching implications for the industrial application of the AnSuR. If the elemental sulfur concentration is high, for example due to poor settleability, relatively more sulfide or a long reaction time is needed to reach a similar effect as opposed to when the total sulfur concentration is lower.

PSD and light microscopy results showed that agglomerates that were initially present in PM2 fell apart 5 min after sulfide addition (Figs. 7 and 8d-f). Noticeably, they were formed again later (at 65 min) in the experiment. The break-up of the agglomerates was not caused by sheer forces from stirring, as the samples had been stirred overnight prior to the experiments. Therefore, we hypothesize that the process was caused by the presence of (poly)sulfide. It is likely that the sulfur dissolution weakened the junctures between the sulfur particles in the agglomerates. By adding sulfide, these junctures were likely to be affected, which enervated the junctions between particles in the agglomerate, causing them to fall apart. It is unclear what caused the re-agglomeration observed at 65 min. A possible explanation for the re-agglomeration is that the surface properties of the biologically produced elemental sulfur particles changed as an effect the nucleophilic dissolution with sulfide. Biologically produced sulfur is more hydrophilic that chemically produced sulfur (Janssen et al., 1996), but due to the nucleophilic dissolution, the surface might have become less hydrophilic. The layer of adsorbed organic groups which caused the hydrophilic properties of the biosulfur could have been partially removed by the nucleophilic dissolution reaction. However, the agglomeration might be different under different stirring conditions. In the BD set-up, particles are mixed by gas bubbles instead of an impeller as in these experiments. Yamaguchi et al. (2021) found that mixing by gas bubbles instead of an impeller limits agglomeration, because agglomerates break down due to gas stirring (Yamaguchi et al., 2021). Thus, the contribution of abiotic agglomeration in the BD set-up could this be less than found in this study. Yet, sulfur particle agglomeration tendency has been shown strong enough as agglomerated sulfur particles have been found on numerous accounts in BD systems despite the gas stirring.

Additionally, the equilibrium reaction between sulfide and polysulfide (Eq. 2) could have continuously provided dissolved S_8, which could have contributed to re-agglomeration as well. However, the rate of this back reaction has not been quantified before (only noted to be very fast by (Teder, 1967)), and would be more likely to take place under pH conditions where the reaction is more thermodynamically viable, generally lower pH conditions (Kafantaris and Druschel, 2020). The mechanism at which S_8 is formed from S_x^{2-} likely proceeds by the hydrolytic cleavage of the reduced sulfane atom. Concerning chain lengths of 8 or lower, it is unknown but unlikely that the same equilibrium reaction takes place, as homocyclic rings of e.g. S_6 and S_7 are unstable under our reaction conditions (Steudel, 1996). In the case that a homocyclic S-ring of 7 or lower would be formed, it would rapidly convert to S_8. To observe if there was any (amorphous) freshly formed sulfur present, it would have been relevant to measure the crystallinity of final product. This would have been interesting as it would provide valuable information about the crystallization process. However, our attempts to measure crystallinity by X-Ray Diffraction in suspension were unsuccessful. We could have measured crystallinity of dried final product, but we did not do this as drying likely would change any amorphous phase of the freshly formed material.

In addition, the dissolution reaction made the surface rougher. Rougher surfaces have been described to be more ideal substrates for particle attachment than smooth surfaces (De Martiń and Ommen, 2013; Katainen et al., 2006). These surface modifications might have stimulated re-agglomeration. Yet, it is remarkable that the sulfur particles of PM1 did not re-agglomerate (Figs. 6 and 8a-c). A likely explanation is the seemingly different crystal structures that were observed from the SEM pictures (Fig. 5): PM1 had more single bipyramidal crystals (which is typical for orthorhombic α-S_8) with smooth surface, although hoppered, whereas PM2 had agglomerates of crystals and rounded particles with an already rougher surface. In general, hoppered growth is characteristic of a high growth rate. However, agglomerated particles are known to grow in an even higher crystallization rate regime. This was described in a previous study: when typical individual bipyramids are formed, the crystals are grown under lower crystallization rates, whereas the agglomerated particles are grown in a higher crystallization rate regime (Mol et al., 2021). Therefore, the sulfur crystals in PM1 were presumably formed at a lower growth rate than those of PM2. Due to being agglomerated, it seemed that PM2 had a higher specific surface area. The higher specific surface area that was already present in the original sample might have amplified agglomeration. It thus seemed like polysulfide formation stimulated re-agglomeration, particularly in particles that were already more agglomerated. Moreover, PM2 was more polydisperse than PM1. Polydisperse particles have a higher agglomeration rate than monodisperse particles, which conceivably contributed to the re-agglomeration that was found for PM2 (Yamaguchi et al., 2021).

An S-shaped curve was found for polysulfide formation, which is typical for autocatalytic reactions (Hartler et al., 1967; Kleinjan et al., 2005a). Moreover, different observed maximum polysulfide formation rates were found. PM1 had an average maximum observed rate of 0.08 mM min^{-1}, whereas the almost the double (0.15 mM min^{-1}) was found for PM2. The different maximum observed rates might be attributed to the more agglomerated particles of PM2 as observed by SEM (Fig. 5). The increased surface area of the agglomerates presumably stimulated polysulfide formation. This is in tandem with other studies that found the same relation between the polysulfide formation rate and the specific surface area (Kafantaris and Druschel, 2020; Avetisyan et al., 2019). However, these studies examined the initial reaction rates of bisulfide with elemental sulfur and did not study the rates under influence of autocatalysis. Hartler et al. and Kleinjan et al. did investigate the autocatalytic reaction and found a surface dependence on the polysulfide formation rate (Hartler et al., 1967; Kleinjan et al., 2005a). The study by Kleinjan et al. is most comparable to our experiments as the experiments therein were also performed with biologically produced

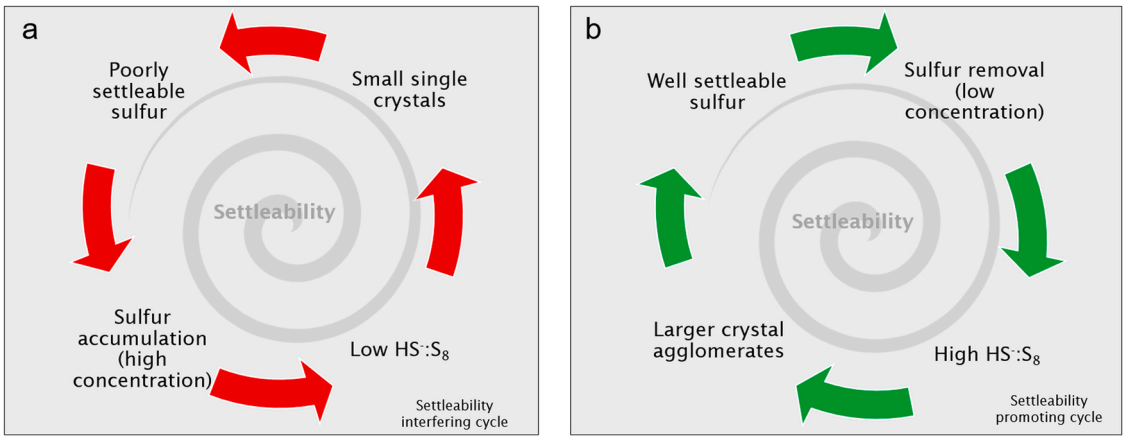

Fig. 12. Processes in the settleability interfering (a) and promoting cycles (b). In the settleability interfering cycle, small single sulfur crystals are poorly settleable, leading to high sulfur concentrations in the reactor system. Thereby the ratio between HS^- and S_8 is low. This in turn produces more poorly settleable small single sulfur crystals. In the settleability promoting cycle, larger crystal agglomerates settle well, leading to a low sulfur concentration in the reactor system. Thereby the ratio between HS^- and S_8 is high. This in turn stimulates crystal agglomeration, leading to good settleability.

sulfur from an industrial BD installation. However, they first removed the largest particles by using settling differences. Therefore, the rates found in our study might be more comparable to rates found in industrial reactors.

The results of our study will help to control the properties of the elemental sulfur produced in BD. The results suggest that the BD process is governed by a set of autocatalytic processes; not only polysulfide formation, but also particle agglomeration and subsequent particle settling (Fig. 12). Single crystals have been shown to have poor settleability, predominantly because they stay small as growing them larger requires sulfur formation rates that are often too low for industrial BD reactors (Mol et al., 2020, 2021). Poor settleability itself also restricts good settleability. Poorly settleable single sulfur crystals accumulate in the process solution, which makes the sulfide-sulfur ratio extremely low and thereby not enough polysulfide is formed to enhance agglomeration. This is described as the 'settleability interfering cycle' (Fig. 12a). On the other hand, agglomeration is stimulating good settleability, as the particle agglomerates show better settleability than single crystals. Moreover, polysulfide formation stimulates settleability as it promotes particle agglomeration and removes the smallest particles in the AnSuR. Good settleability itself is also promoting settleability. When the sulfur had good settleability, the total sulfur concentration in the process solution will be low, leading to high sulfide-sulfur ratios. In this way enough polysulfide may be formed to stimulate agglomeration. This is described as the 'settleability promoting cycle' (Fig. 12b). The settleability promoting processes are stimulated by the added AnSuR. This implies that when the AnSuR is added, the instigated processes will stimulate a good particle settleability. For practical implementation, the sulfide-sulfur ratio should be high enough and the retention time should be long enough. Models and additional experimental work could help define these boundaries.

As the sulfur particles are continuously formed and dissolved in the overall process, it is not expected that their size remains the same throughout the entire retention time in the reactor system. However, when the particles have grown large enough, they will be removed with a settler or decanter centrifuge, and after this recovery step, the particle size is no longer important for process operation. Particle size distribution of a sample in suspension remained stable for 3 years at 4 °C, and dried samples stayed visibly unchanged (data not shown).

5. Conclusion

We performed batch reactor sulfur dissolution experiments on two different biologically produced elemental sulfur samples from industrial BD installations, one with loose crystals and one with agglomerated crystals. We simulated the effect of the AnSuR on the sulfur particle morphology and size distribution by the addition of sulfide. We found that dissolution of elemental sulfur by (poly)sulfide changed the particle size distribution and morphology. The surface became coarser and more porous, and small individual particles completely disappeared. Agglomerates fell apart in the beginning of the equilibrium reaction but, depending on initial morphology, were formed again likely as a result of the dissolution reaction. Thus, we have found a method to increase the size of biologically formed sulfur particles. To our best knowledge this is the first time that polysulfide formation is used to enhance agglomeration of sulfur to improve settleability. Moreover, we discovered that for each sample the morphology and particle size change happened at a different observed maximum polysulfide formation rate. For practical implementation of the dissolution reaction to remove small particles and induce agglomeration, the sulfide-sulfur ratio should be high enough and the retention time should be long enough. Hereby we show that these changes occurred purely due to abiotic reactions and were not caused by biological (poly)sulfide oxidation. If we can use the method from this study to control the particle size, the BD process can be optimized. This innovation applies to an already existing and industrialized process, which adds largely to the scope at which the innovation will be applied.

Funding

This work was financed by Paqell B.V, The Netherlands.

CRediT authorship contribution statement

Annemerel R. Mol: Formal Analysis, Investigation, Writing – original draft, Visualization. **Lourens J. van Langeveld:** Methodology, Formal analysis, Investigation, Writing – review & editing, Visualization. **Renata D. van der Weijden:** Conceptualization, Writing – review & editing, Supervision. **Johannes B.M. Klok:** Conceptualization, Writing – review & editing, Supervision, Project administration. **Cees J. N. Buisman:** Conceptualization, Writing – review & editing, Supervision, Funding acquisition.

Declaration of Competing Interest

The authors declare that they have no known competing financial interests or personal relationships that could have appeared to influence the work reported in this paper.

Acknowledgement

We thank Marcel Giesbers from the Wageningen Electron Microscopy Centre for taking SEM pictures.

Appendix A. Supporting information

Supplementary data associated with this article can be found in the online version at doi:10.1016/j.jhazmat.2021.127696.

References

Avetisyan, K., Buchshtav, T., Kamyshny, A., 2019. Kinetics and mechanism of polysulfides formation by a reaction between hydrogen sulfide and orthorhombic cyclooctasulfur. Geochim. Cosmochim. Acta 247, 96–105. https://doi.org/10.1016/j.gca.2018.12.030.

Banciu, H., Sorokin, D.Y., Kleerebezem, R., Muyzer, G., Galinski, E.A., Kuenen, J.G., 2004. Growth kinetics of haloalkaliphilic, sulfur-oxidizing bacterium Thioalkalivibrio versutus strain ALJ 15 in continuous culture. Extremophiles 8, 185–192. https://doi.org/10.1007/s00792-004-0376-5.

Buisman, C.J., Geraats, B.G., Ijspeert, P., Lettinga, G., 1990. Optimization of sulphur production in a biotechnological sulphide-removing reactor. Biotechnol. Bioeng. 35, 50–56. https://doi.org/10.1002/bit.260350108.

Ceradis Crop Protection, Cerasulfur SC, (2021). ⟨https://ceradis.com/products/crop-protection/cerasulfur-sc/⟩ (accessed March 30, 2021).

Danielsson, L.G., Chai, X.S., Behm, M., Renberg, L., 1996. UV characterization of sulphide-polysulphide solutions and its application for process monitoring in the electrochemical production of polysulphides. J. Pulp Pap. Sci. 22, J187–J191.

De Martiń, L., Ommen, J.R.Van, 2013. A model to estimate the size of nanoparticle agglomerates in gas-solid fluidized beds. J. Nanopart. Res. 15, 1–9. https://doi.org/10.1007/s11051-013-2055-x.

De Rink, R., Klok, J.B.M., Van Heeringen, G.J., Sorokin, D.Y., Heijne, A., Zeijlmaker, R., Mos, Y.M., De Wilde, V., Keesman, K.J., Buisman, C.J.N., 2019. Increasing the selectivity for sulfur formation in biological gas desulfurization. Environ. Sci. Technol. 53, 4519–4527. https://doi.org/10.1021/acs.est.8b06749.

Desarnaud, J., Derluyn, H., Carmeliet, J., Bonn, D., Shahidzadeh, N., 2018. Hopper growth of salt crystals. J. Phys. Chem. Lett. 9, 2961–2966. https://doi.org/10.1021/acs.jpclett.8b01082.

Fertipaq Natural Solutions, Fertipaq, (2021). ⟨https://en.fertipaq.com/⟩ (Accessed 30 March 2021).

Ghosh, W., Dam, B., 2009. Biochemistry and molecular biology of lithotrophic sulfur oxidation by taxonomically and ecologically diverse bacteria and archaea. FEMS Microbiol. Rev. 33, 999–1043. https://doi.org/10.1111/j.1574-6976.2009.00187.x.

González-Cortés, J.J., Torres-Herrera, S., Almenglo, F., Ramírez, M., Cantero, D., 2021. Anoxic biogas biodesulfurization promoting elemental sulfur production in a continuous stirred tank bioreactor. J. Hazard. Mater. 401, 123785 https://doi.org/10.1016/j.jhazmat.2020.123785.

Hartler, N., Libert, J., Teder, A., 1967. Rate of sulfur dissolution sodium sulfide in aqueous sodium sulfide. Ind. Eng. Chem. Process Des. Dev. 6, 398–406. https://doi.org/10.1021/i260024a002.

Janssen, A.J.H., De Keizer, A., Van Aelst, A., Fokkink, R., Yangling, H., Lettinga, G., 1996. Surface characteristics and aggregation of microbiologically produced sulphur particles in relation to the process conditions. Colloids Surf. B Biointerfaces 6, 115–129. https://doi.org/10.1016/0927-7765(95)01246-X.

Janssen, A.J.H., Meijer, S., Bontsema, J., Lettinga, G., 1998. Application of the redox potential for controlling a sulfideoxidizing bioreactor. Biotechnol. Bioeng. 60, 147–155. https://doi.org/10.1002/(SICI)1097-0290(19981020)60:2<147::AID-BIT2>3.0.CO;2-N.

Janssen, A.J.H., Ruitenberg, R., Buisman, C.J.N., 2001. Industrial applications of new sulphur biotechnology. Water Sci. Technol. 44, 85–90. https://doi.org/10.2166/wst.2001.0471.

Janssen, A.J.H., Lens, P.N.L., Stams, A.J.M., Plugge, C.M., Sorokin, D.Y., Muyzer, G., Dijkman, H., Van Zessen, E., Luimes, P., Buisman, C.J.N., 2009. Application of bacteria involved in the biological sulfur cycle for paper mill effluent purification. Sci. Total Environ. 407, 1333–1343. https://doi.org/10.1016/j.scitotenv.2008.09.054.

Kafantaris, F.C.A., Druschel, G.K., 2020. Kinetics of the nucleophilic dissolution of hydrophobic and hydrophilic elemental sulfur sols by sulfide. Geochim. Cosmochim. Acta 269, 554–565. https://doi.org/10.1016/j.gca.2019.11.010.

Kamyshny, A., Goifman, A., Rizkov, D., Lev, O., 2003. Kinetics of disproportionation of inorganic polysulfides in undersaturated aqueous solutions at environmentally relevant conditions. Aquat. Geochem. 9, 291–304. https://doi.org/10.1023/B:AQUA.0000029023.07252.c3.

Kamyshny, A., Gun, J., Rizkov, D.A.N., Voitsekovski, T., Lev, O., 2004. Equilibrium distribution of polysulfide ions in aqueous solutions at different temperatures by rapid single phase derivatization. Environ. Sci. Technol. 41, 2395–2400.

Katainen, J., Paajanen, M., Ahtola, E., Pore, V., Lahtinen, J., 2006. Adhesion as an interplay between particle size and surface roughness. J. Colloid Interface Sci. 304, 524–529. https://doi.org/10.1016/j.jcis.2006.09.015.

Kiragosyan, K., Klok, J.B.M., Keesman, K.J., Roman, P., Janssen, A.J.H., 2019. Development and validation of a physiologically based kinetic model for starting up and operation of the biological gas desulfurization process under haloalkaline conditions. Water Res. X. 4, 100035 https://doi.org/10.1016/j.wroa.2019.100035.

Kiragosyan, K., Picard, M., Timmers, P.H.A., Sorokin, D.Y., Klok, J.B.M., Roman, P., Janssen, A.J.H., 2020. Effect of methanethiol on process performance, selectivity and diversity of sulfur-oxidizing bacteria in a dual bioreactor gas biodesulfurization system. J. Hazard. Mater. 398, 123002 https://doi.org/10.1016/j.jhazmat.2020.123002.

Kleinjan, W.E., De Keizer, A., Janssen, A.J.H., 2005a. Kinetics of the reaction between dissolved sodium sulfide and biologically produced sulfur. Ind. Eng. Chem. Res. 44, 309–317.

Kleinjan, W.E., De Keizer, A., Janssen, A.J.H., 2005b. Equilibrium of the reaction between dissolved sodium sulfide and biologically produced sulfur. Colloids Surf. B Biointerfaces 43, 228–237. https://doi.org/10.1016/j.colsurfb.2005.05.004.

Lide, D.R., 2005. CRC Handbook of Chemistry and Physics, Internet V. CRC Press, Boca Raton, FL.

Mol, A.R., Meuwissen, D.J.M., Pruim, S.D., Zhou, C., van Vught, V., Klok, J.B.M., Buisman, C.J.N., van der, R.D.Weijden., 2021. Novel agglomeration strategy for elemental sulfur produced during biological gas desulfurization. ACS Omega 6 (42), 27913–27923. https://doi.org/10.1021/acsomega.1c03701.

Mol, A.R., Van Der Weijden, R.D., Klok, J.B.M., Buisman, C.J.N., 2020. Properties of sulfur particles formed in biodesulfurization of biogas. Minerals 10, 433. https://doi.org/10.3390/min10050433.

Muyzer, G., Sorokin, D.Y., Mavromatis, K., Lapidus, A., Clum, A., Ivanova, N., Pati, A., D'Haeseleer, P., Woyke, T., Kyrpides, N.C., 2011. Complete genome sequence of "Thioalkalivibrio sulfidophilus" HL-EbGr7. Stand. Genom. Sci. 4, 23–35. https://doi.org/10.4056/sigs.1483693.

Roman, P., Bijmans, M.F.M., Janssen, A.J.H., 2014. Quantification of individual polysulfides in lab-scale and full-scale desulfurisation bioreactors. Environ. Chem. 11, 702. https://doi.org/10.1071/en14128.

Sorokin, D.Y., Banciu, H., Van Loosdrecht, M., Kuenen, G.J., 2003. Growth physiology and competitive interaction of obligately chemolithoautotrophic, haloalkaliphilic, sulfur-oxidizing bacteria from soda lakes. Extremophiles 7, 195–203. https://doi.org/10.1007/s00792-002-0313-4.

Sorokin, D.Y., Van Den Bosch, P.L.F., Abbas, B., 2008. Microbiological analysis of the population of extremely haloalkaliphilic sulfur-oxidizing bacteria dominating in lab-scale sulfide-removing bioreactors. Appl. Microbiol. Biotechnol. 80, 965–975. https://doi.org/10.1007/s00253-008-1598-8.

Steudel, R., 1996. Mechanism for the formation of elemental sulfur from aqueous sulfide in chemical and microbiological desulfurization processes. Ind. Eng. Chem. Res. 35, 1417–1423.

Teder, A., 1967. Spectrophotometric determination of polysulfide excess sulfur in aqueous solutions. Sven. Papp. 6, 197–200.

Van Den Bosch, P.L.F., De Graaff, M., Fortuny-picornell, M., Van Leerdam, R.C., Janssen, A.J.H., 2009. Inhibition of microbiological sulfide oxidation by methanethiol and dimethyl polysulfides at natron-alkaline conditions. Appl. Microbiol. Biotechnol. 83, 579–587. https://doi.org/10.1007/s00253-009-1951-6.

Van Zessen, E., Janssen, A.J.H., De Keizer, A., Heine, B., Peace, J., Abry R. (2004). Application of THIOPAQ TM biosulphur in agriculture, Proc. Br. Sulphus Events 2004 Sulphur Conf. Barcelona, Spain, 24–27 Oct. 2004, 57–68.

Yamaguchi, A., Okano, H., Sumitomo, S., Uddin, M.A., Kato, Y., 2021. Effect of impeller and gas stirring on agglomeration behavior of polydisperse fine particles in liquid. ISIJ Int. 61, 1775–1783. https://doi.org/10.2355/isijinternational.ISIJINT-2020-688.